Reactions of Laser-Ablated Chromium Atoms, Cations, and Electrons with CO in Excess Argon and Neon: Infrared Spectra and Density Functional Calculations on Neutral and Charged Unsaturated Chromium Carbonyls

Lester Andrews,* Mingfei Zhou,† Gennady L. Gutsev, and Xuefeng Wang

Chemistry Department, P.O. Box 400319, University of Virginia, Charlottesville, Virginia 22904-4319

Received: September 10, 2002; In Final Form: October 31, 2002

Laser-ablated Cr atoms react with CO ($^{12}C^{16}O$, $^{13}C^{16}O$, $^{12}C^{18}O$) in excess argon to give the same $Cr(CO)_{3,4,5}$ species observed from the photodissociation of $Cr(CO)_6$. Similar reactions in excess neon give neon matrix fundamentals between argon matrix and gas-phase values. The dicarbonyl $Cr(CO)_2$ is bent with 1970.8, 1821.5 cm^{-1} and 1982.1, 1832.9 cm^{-1} C−O stretching fundamentals in solid argon and neon, respectively. The high-spin CrCO molecule appears at 1975.6 and 2018.4 cm^{-1} in solid argon and neon, respectively, and exhibits a strong matrix interaction. The $CrCO^+$ cation and $Cr(CO)_2^-$ anion are observed in laser-ablation experiments in solid neon at 2200.7 and 1705.0 cm^{-1}, respectively. The $Cr_2(CO)_2$ complex absorbs strongly at 1735.4 cm^{-1} and gives several combination bands in neon. Density functional theory calculations support the vibrational assignments.

Introduction

Coordinatively unsaturated transition-metal carbonyls are active species in catalytic reactions and are building blocks for stable organometallic complexes.[1−3] Chromium carbonyl intermediates were investigated early owing to the availability of the $Cr(CO)_6$ precursor molecule. Unsaturated chromium carbonyls were studied first in rare-gas matrices[4−10] and then in solution[11] and the gas phase by the photodissociation of $Cr(CO)_6$.[12−14] The Turner group produced the penta-, tetra-, and tricarbonyls in rare-gas matrices for characterization by infrared spectroscopy.[4,6−9] The pentacarbonyls were found to have the C_{4v} structure, whereas C_{2v} and C_{3v} structures were determined for the tetra- and tricarbonyls. Time-resolved infrared absorption studies by the Weitz,[12] Rosenfeld,[13] and Rayner[14] groups provided evidence that the unsaturated photolysis products adopt the same structures in the gas phase. The latter investigations also found that bimolecular rate constants for CO addition to $Cr(CO)_n$ ($n = 3-5$) are within an order of magnitude of the gas kinetic collision rate, indicating that the ground states of the tri-, tetra-, and pentacarbonyls all have the same singlet spin state. The photodissociation of $Cr(CO)_6$ continues to attract a lot of attention. Primary and secondary photoproducts have been observed by mass spectrometry,[15] and vibrational relaxation dynamics in the picosecond and femtosecond time ranges have been recently investigated.[16,17]

The simple CrCO complex was characterized by Weltner and co-workers, who reported a 1977 cm^{-1} absorption from the reaction of thermal Cr atoms and CO diluted in argon.[10] Laser-ablated Cr with CO gave a 1975.3 cm^{-1} argon matrix absorption in more recent experiments.[18] The CrCO molecule was predicted to have a $^7A'$ ground state, which correlates with the ground-state Cr atom (^7S) and CO ($^1\Sigma^+$).[19−21] Interestingly, the ground-state CrCO molecule adopts a bent geometry.[19] The 5σ orbital of CO does not point directly toward the metal in bent CrCO, and the σ repulsion can be reduced; this repulsion, coupled with the fact that sdσ hybridization is not possible for the ^7S state of Cr due to the spin coupling of the s and dσ orbitals, acts as a driving force for bending.[19,21,22]

We report here a combined argon- and neon-matrix infrared experimental and density functional theoretical investigation of the unsaturated chromium carbonyls, with emphasis on the smaller coordination numbers and the new neon matrix observations particularly for charged species. In these laser-ablation experiments, metal atoms, cations, and electrons are produced,[22] and several charged metal carbonyl species are also trapped.

Experimental and Computational Methods

The experimental method for laser ablation and matrix isolation has been described in detail previously.[23−25] Briefly, the Nd:YAG laser fundamental (1064 nm, 10 Hz repetition rate with 10 ns pulse width) was focused onto the rotating chromium target (Johnson-Matthey, 99.2%). Typically, low laser power (3−5 mJ/pulse) was used, which favors the stabilization of ionic species and minimizes cluster formation. Laser-ablated metal atoms, cations, and electrons were co-deposited with carbon monoxide (0.05−0.4%) in excess argon or neon onto a 10 or 4 K CsI cryogenic window at 2−4 mmol/h for 0.5−1 h. Carbon monoxide (Matheson) and isotopic $^{13}C^{16}O$ and $^{12}C^{18}O$ (Cambridge Isotopic Laboratories) and selected mixtures were used in different experiments. Infrared spectra were recorded at 0.5 cm^{-1} resolution on a Nicolet 750 spectrometer with 0.1 cm^{-1} accuracy using a mercury cadmium telluride detector down to 400 cm^{-1}. Matrix samples were annealed at different temperatures, and selected samples were subjected to photolysis using a medium-pressure mercury lamp ($\lambda > 240$ nm) with the globe removed.

Density functional theory (DFT) calculations were performed on all of the proposed reaction products using the Gaussian 98 program.[26] Two generalized gradient approximations consisting of combinations of Becke's exchange and Perdew's correlation (BP86) and Becke's exchange and Perdew−Wang's correlation

* Corresponding author. E-mail: lsa@virginia.edu.
† Present address: Department of Chemistry, Fudan University, Shanghai 200433, People's Republic of China.

10.1021/jp026955g CCC: $25.00
Published on Web 01/01/2003

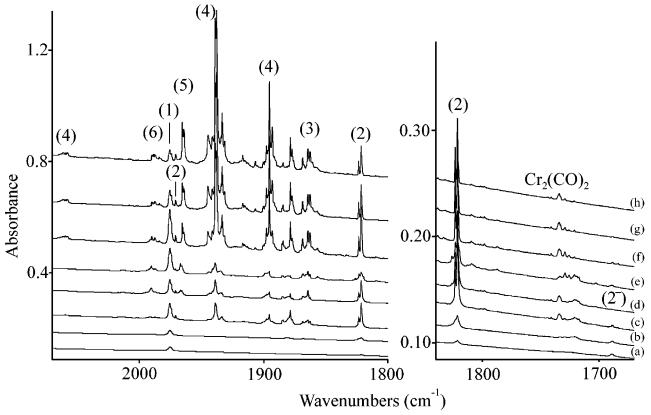

Figure 1. Infrared spectra in the 2070−1800 and 1830−1680 cm^{-1} regions for reduced-energy laser-ablated Cr co-deposited with 0.2% CO in argon at 10 K. Sample deposited (a) for 60 min, (b) after annealing to 20 K, (c) after annealing to 25 K, (d) after $\lambda > 470$ nm photolysis for 15 min, (e) after $\lambda > 240$ nm photoylsis, (f) after annealing to 30 K, (g) after annealing to 35 K, and (h) after annealing to 40 K. The label gives the number of carbonyl ligands coordinated to a single Cr atom.

(BPW91) functionals[27] as well as the hybrid Hartree−Fock B3LYP functional[28] were chosen. The 6-311+G* basis set was used for carbon and oxygen,[29] and the all-electron Wachters−Hay[30] basis as modified by Gaussian was used for chromium.

Results

Infrared spectra of the chromium carbonyl products formed by the reaction of laser-ablated metal and CO in excess argon and neon and DFT calculations of potential product states, energies, and frequencies will be presented.

Cr and CO in Argon. Experiments were done using 0.4 and 0.2% CO in argon, and the latter using 10% of the laser energy of the former is illustrated in Figure 1. The weak 1975.6 cm^{-1} band is in agreement with two previous assignments to CrCO. Two still weaker bands are found at 1821.5 and 1688.0 cm^{-1}. Annealing to 20 K markedly increased the 1821.5 cm^{-1} adsorption and a broad 1721 cm^{-1} feature with little effect on the 1975.6- and 1688.0 cm^{-1} bands (Figure 1b). Annealing to 25 K increased all but the latter band: the CrCO band at 1975.6 cm^{-1} increased 3×, the sharp 1821.5 cm^{-1} feature increased 5× and found a relative at 1970.8 cm^{-1}, and the 1721 cm^{-1} band and 1734 cm^{-1} satellite increased markedly while new features appeared at 1938.7, 1895.3, 1878.5, and 1864.5 cm^{-1} (Figure 1c). The latter is in agreement with the Turner group's assignment[8,9] to $Cr(CO)_3$, and the former two match $Cr(CO)_4$ bands produced from the photodissociation of $Cr(CO)_6$. The sharp new 1878.5 cm^{-1} feature decreases 75% on $\lambda > 470$ nm radiation, whereas the 1688.0 cm^{-1} band disappears and new 1967.0- and 1990.4 cm^{-1} absorptions appear (Figure 1d). The latter are due to $Cr(CO)_5$ and $Cr(CO)_6$.[6−9] Next, full-arc irradiation increases 1967.0 cm^{-1} at the expense of 1990.4 cm^{-1} and the other absorptions save CrCO, which appears to be stable; in addition, some 1668.0 cm^{-1} absorption is regenerated, and a weak 1857.6 cm^{-1} absorption is produced (Figure 1e). A subsequent annealing to 30 K affects major growth in the 1970.8, 1821.5 cm^{-1} and 1938.7, 1895.3 cm^{-1} absorptions and the 1878.5 and 1864.5 cm^{-1} bands (Figure 1f). The next annealing to 35 K decreases CrCO, the 1970.8, 1821.5 cm^{-1} pair, the 1734.0 cm^{-1} feature, and the 1688.0 cm^{-1} band, and slightly increases the remaining absorptions (Figure 1g). The final annealing to 40 K continues this trend (Figure 1h). Lower-frequency product absorptions are given in Table 1.

TABLE 1: Infrared Absorptions (cm^{-1}) from Codeposition of Laser-Ablated Cr with CO in Excess Argon

^{12}CO	^{13}CO	$^{12}CO + {}^{13}CO$[a]	$^{12}CO/^{13}CO$	assignment
2058.5	2013.8	2044.1, 2028.7, 2023.8	1.0222	$Cr(CO)_4$, a_1
1990	1946		1.0226	$Cr(CO)_6$
1975.6	1932.8		1.0221	CrCO
1970.8	1925.7	1951.3	1.0234	$Cr(CO)_2$, a_1
1967.0	1923.9		1.0224	$Cr(CO)_5$, e
1965.4	1922.2		1.0225	$Cr(CO)_5$, e
1944.7	1902.3		1.0223	$Cr(CO)_4$ site
1938.7	1896.4	1917.7, 1906.0	1.0223	$Cr(CO)_4$, b_2
1933.3	1889.2	1927.7	1.0233	$Cr(CO)_4$, a_1
1916.8	1874.8		1.0224	$Cr_x(CO)_y$
1906.6	1864.9		1.0224	$Cr_x(CO)_y$
1895.3	1852.3	1865.1	1.0232	$Cr(CO)_4$, b_1
1893.0	1850.0		1.0232	$Cr(CO)_4$ site
1878.5	1837.7		1.0222	$Cr_x(CO)$
1868.5	1825.9		1.0233	$Cr(CO)_3$ site
1864.5	1821.8	1846, 1833	1.0234	$Cr(CO)_3$, e
1862.6	1820.1		1.0234	$Cr(CO)_3$ site
1856.7	1815.2		1.0229	$Cr(CO)_5$-
1823.4	1783.1	1800.8	1.0230	$Cr(CO)_2$ site
1821.5	1781.3	1798.4	1.0226	$Cr(CO)_2$, b_2
1809.6	1769.0		1.0230	$Cr_x(CO)_y$
1798.3	1759.6		1.0222	$Cr_x(CO)_y$
1741.1	1703.3		1.0222	$Cr_2(CO)_2$ site
1734.0	1697.3	1714.0	1.0216	$Cr_2(CO)_2$
1721.1	1685.4	1702	1.0212	$Cr_2(CO)_2$ site
1688.9	1650.6	1666.5		$Cr(CO)_2^-$
1688.0	1649.6	1665.5	1.0233	$Cr(CO)_2^-$
680.8				$Cr(CO)_3$
670.1	656.8			$Cr(CO)_6$
654.7	639.8			?
647.3	632			$Cr(CO)_5$?
637.1	621.4		1.0253	$Cr(CO)_4$
603.1	591.6		1.019.4	$Cr(CO)_5$
549.1				$Cr(CO)_4$?
483				$Cr(CO)_3$
453.7	451.0			$Cr(CO)_5$
433.3				$Cr(CO)_4$

[a] New bands with an isotopic mixture.

The experiment with 10× higher laser energy gave stronger absorptions. However, the 1916.8, 1906.6, and 1878.6 cm^{-1} features were enhanced, and the 1688.0 cm^{-1} band was diminished relative to the others.

Two experiments were done with 0.2% ^{13}CO in argon using different photolysis wavelengths. The product bands behave like the ^{12}CO bands on annealing, and the absorptions are listed in Table 1. Photolysis ($\lambda > 800$ nm) destroyed the 1837.8 cm^{-1} band (counterpart to 1878.5 cm^{-1}) and the 1875.8 cm^{-1} band (counterpart to 1916.8 cm^{-1}) and halved the 1649.6 cm^{-1} band (counterpart to 1688.0 cm^{-1}).

Finally, an experiment with mixed ^{12}CO and ^{13}CO gave diagnostic multiplets, which identify the CO stoichiometries of the product complexes, and spectra are shown in Figure 2. The co-deposition spectrum reveals a 1975.8−1932.8 cm^{-1} doublet for CrCO, as reported previously,[10] and a weak triplet at 1821.5−1798.4−1781.3 cm^{-1}, which increases on subsequent annealing and indicates two equivalent CO subunits. The weaker associated 1970.8−1951.3−1925.7 cm^{-1} triplet is apparent after annealing.

The sharp 1864.5 cm^{-1} band with site splittings at 1868.5 and 1862.6 cm^{-1} is in agreement with the Turner group's assignment to $Cr(CO)_3$ with C_{3v} structure.[8] The $Cr(^{13}CO)_3$ counterpart at 1821.6 cm^{-1} defines a $^{12}CO/^{13}CO$ ratio of 1.0234, which is appropriate for a C−O vibration. After $\lambda > 470$ nm photolysis, when $Cr(CO)_3$ increases more than other products absorbing in this region, two weaker intermediate bands are

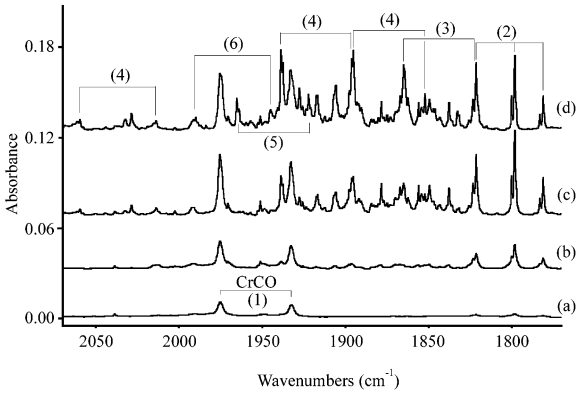

Figure 2. Infrared spectra in the 2070−1770 cm^{-1} region for laser-ablated Cr co-deposited with mixed 0.1% ^{12}CO and 0.08% ^{13}CO in argon at 10 K. Sample deposited (a) for 60 min, (b) after annealing to 20 K, (c) after annealing to 25 K, and (d) after annealing to 30 K.

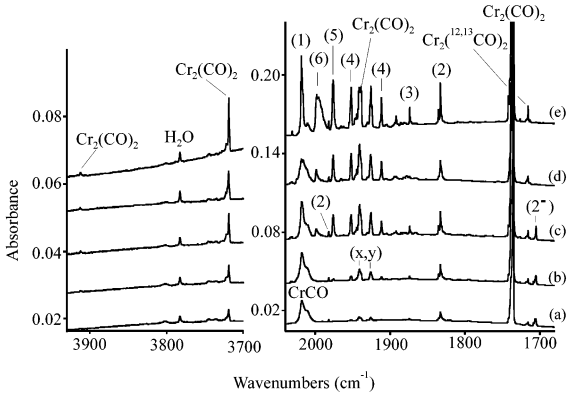

Figure 3. Infrared spectra in the 3930−3700 and 2040−1680 cm^{-1} regions for reduced-energy laser-ablated Cr co-deposited with 0.1% CO in neon at 4 K. Sample deposited (a) for 30 min, (b) after annealing to 6 K, (c) after annealing to 8 K, (d) after $\lambda > 240$ nm photolysis for 15 min, and (e) after annealing to 10 K.

observed at 1846 and 1833 cm^{-1}, which provide the signature for the doubly degenerate vibration of a trigonal species (Figure 2d).[31]

The bands observed here at 1938.7 and 1895.3 cm^{-1} show the same 2:1 intensity ratio as the 1938 and 1891 cm^{-1} bands assigned by the Turner group[8] to $Cr(CO)_4$. We note their concern that absorption at 1896 cm^{-1} may be due to a higher carbonyl, but our 1895.3 cm^{-1} band is sharp and maintains a constant relative intensity with the 1938.7 cm^{-1} band, so both appear to be due to $Cr(CO)_4$ in our argon matrix. Between the two strong b_2 modes for $Cr(^{12}CO)_4$ and $Cr(^{13}CO)_4$ at 1938.7 and 1896.4, we observe two weaker mixed-isotope bands at 1917.7 and 1906.0 cm^{-1}, and between the two weaker b_1 modes for $Cr(^{12}CO)_4$ and $Cr(^{13}CO)_4$ at 1895.3 and 1852.3 cm^{-1}, we observe one strong intermediate band at 1865.1 cm^{-1}.

Our sharp 1965.4 cm^{-1} band is in agreement with the 1966 cm^{-1} band conclusively assigned to the strong (e) mode of $Cr(CO)_5$ by the Turner group.[9] We note that $Cr(CO)_5$ made by photolysis absorbs here at 1967.0 cm^{-1} and that $Cr(CO)_5$ formed by reactions of CO on annealing absorbs at 1965.4 cm^{-1}. We observe no intermediate mixed-isotope components as absorptions for other species mask this region.

Cr + CO in Neon. The neon matrix spectrum is complementary to the argon matrix spectrum, but it must be remembered that neon condenses more slowly at 4 K and does not trap reactive species as efficiently as argon at 10 K, except sometimes in the case of charged species. On deposition, the neon matrix spectrum reveals much stronger absorptions than the argon matrix, most notably the very strong absorption at 1735.4 cm^{-1} with ^{12}CO, the ^{13}CO counterpart in natural abundance at 1715.6 cm^{-1} (Figure 3). The new sharp 1705.0 cm^{-1} absorption is about twice as intense as its 1688.0 cm^{-1} argon matrix counterpart. Very weak 1762.9 and 1678.0 cm^{-1} absorptions are also observed. The new band at 2018.4 cm^{-1} is of comparable absolute intensity to the 1975.6 cm^{-1} argon matrix CrCO band, but the sharp 1832.9 cm^{-1} absorption is stronger than the 1821.5 cm^{-1} argon matrix counterpart, and the associated weaker 1982.1 cm^{-1} absorption is observed on deposition. In addition, sharp, weak 1952.2, 1911.4, and 1873.8 cm^{-1} bands and broader 1940.9, 1926.0 cm^{-1} features were observed, whose counterparts were not produced in argon until annealing. In the case of the broader bands, high annealing produced weak argon matrix counterparts at 1916.8 and 1906.6 cm^{-1}. Next annealing the neon matrix to 6 K slightly increased all of the above bands and produced a weak new 1976.2 cm^{-1} absorption (Figure 3b). Subsequent annealing to 8 K produced little increase in the first 2018.4 and 1832.9 cm^{-1} bands, a marked increase in the 1976.2, 1952.2, 1940.9, 1926.0, 1911.4, and 1873.8 cm^{-1} bands, a new 1998.8 cm^{-1} absorption, which is due to $Cr(CO)_6$, based on its proximity to the 2002.4 cm^{-1} gas-phase absorption,[32] and a new 1892.0 cm^{-1} band (Figure 3c). The upper region contains weak 3912.4 and 3718.8 cm^{-1} bands that track with the very strong 1735.4 cm^{-1} band on annealing and in other experiments. The relative absorbances are 0.0008, 0.016, and 0.518. The sharp 1938.6 cm^{-1} shoulder also tracks with these bands and gives an approximate relative absorbance of 0.01.

Full-arc photolysis broadens the 2018.4 cm^{-1} absorption, slightly increases bands in the 1900 cm^{-1} region, and destroys the 1762.9, 1705.0, and 1678.0 cm^{-1} absorptions (Figure 3d). (In another experiment, the latter bands were destroyed by $\lambda >$ 470 nm photolysis.) A final annealing to 10 K sharpened the 2018.4 cm^{-1} absorption, markedly increased the $Cr(CO)_6$ band, almost doubled the 1976.2 cm^{-1} band, slightly increased the other bands (save for 1940.9 cm^{-1}), and markedly increased the 1892.0 cm^{-1} band.

A sharp, weak doublet at 2200.7, 2199.2 cm^{-1} and a weak 2178.1 cm^{-1} band increase on annealing to 8 K, reaching absorbances of 0.007 and 0.0003, respectively, and are destroyed on full-arc photolysis. An identical experiment with 0.1% CO and 0.02% CCl_4 to serve as an electron trap[22,33] gave a substantially stronger 2200.7, 2199.2 cm^{-1} doublet on deposition, and this doublet increased 2-fold on annealing to 8 K, reaching 3 times the absorbance of the comparable spectrum without CCl_4, and the 2178.1 cm^{-1} band reached 0.001 absorbance (Figure 4). In addition, a very weak 2172.2 cm^{-1} band was enhanced with CCl_4, and new features appeared at 2167.6 and 2162.0 cm^{-1} (on top of a 2160.2 cm^{-1} band due to a $(CO)_x$ species). The 2018.4 cm^{-1} (CrCO) and 1832.9 cm^{-1} ($Cr(CO)_2$) absorptions were half and the 1762.9, 1705.0, and 1678.0 cm^{-1} bands were <5% of their original intensities without CCl_4 present.

Another experiment was performed with reduced laser energy using 0.05% CO, and the 2018.4 and 1832.9 cm^{-1} absorption were 20 and 5% as strong as in Figure 3a, respectively, but the 1735.4 cm^{-1} band was 4% as intense, and the 3718.8 cm^{-1} band followed suit. The 1873.8 cm^{-1} band was detected, but other bands in this region were produced by annealing.

Isotopic substitution was done with $^{13}C^{16}O$ and $^{12}C^{18}O$ using identical conditions, and the spectra appeared the same as shown in Figure 3, but the bands were shifted as reported in Table 2. A ^{13}CO sample was doped with CCl_4, and the sharp 2151.9,

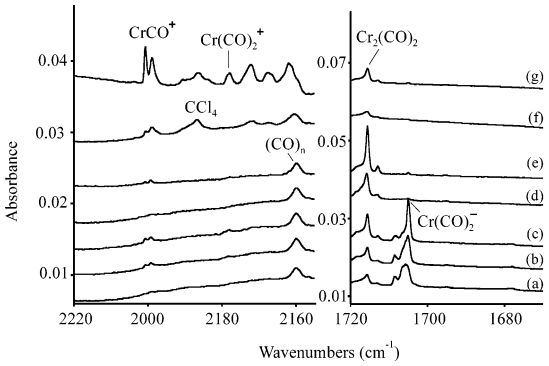

Figure 4. Infrared spectra in the 2220−2155 and 1720−1670 cm^{-1} regions for laser-ablated chromium co-deposited with 0.1% CO in neon at 4 K. Sample deposited (a) for 30 min, (b) after annealing to 6 K, (c) after annealing to 8 K, (d) after $\lambda > 240$ nm photolysis, (e) after annealing to 10 K, (f) for 30 min, with 0.02% CCl_4 added, and (g) after annealing to 12 K.

TABLE 2: Infrared Absorptions (cm^{-1}) from Codeposition of Laser-Ablated Cr with the CO Molecule in Excess Neon

$^{12}C^{16}O$	$^{13}C^{16}O$	$^{12}C^{18}O$	R(12/13)	*R*(16/18)	assignment
3912.4	3835.0	3821.2	1.0202	1.0239	$Cr_2(CO)_2$ comb
3718.8	3637.4	3633.9	1.0224	1.0234	$Cr_2(CO)_2$ comb
2200.7	2151.9	2148.9	1.0227	1.0241	$CrCO^+$
2199.2	2150.1	2147.8	1.0228	1.0239	$CrCO^+$ site
2178.1	2129.8	2126.8	1.0227	1.0241	$Cr(CO)_2^+$
2172.2	2123.5		1.0229		$(Cr(CO)_3^+)$
2140.8	2093.7	2098.7	1.0225	1.0245	CO
2066.1	2018.2	2018.3	1.0237	1.0237	$Cr(CO)_4$, a_1
2056.3	2010.9	2007.4	1.0226	1.0244	$(CO)_2^+$
2030.9	1986.3	1982.7	1.0225	1.0243	CrCO site
2018.4	1974.6	1969.8	1.0222	1.0248	CrCO
1998.8	1954.1	1951.2	1.0229	1.0244	$Cr(CO)_6$
1982.1	1937.0	1937.4	1.0233	1.0231	$Cr(CO)_2$, a_1
1976.2	1932.2	1929.2	1.0228	1.0244	$Cr(CO)_5$
1952.2	1909.4	1905.5	1.0224	1.0245	$Cr(CO)_4$, b_2
1940.9	1898.9	1894.7	1.0221	1.0244	$Cr_x(CO)_y$
1938.6	1896.5	1892.4	1.0222	1.0244	$Cr_2(CO)_2$ comb
1926.0	1883.1	1880.8	1.0228	1.0240	$Cr_x(CO)_y$
1911.4	1868.1	1868.3	1.0232	1.0231	$Cr(CO)_4$, b_1
1892.0	1850.0	1847.9	1.0227	1.0239	$Cr_x(CO)_y$
1873.8	1831.5	1831.2	1.0231	1.0233	$Cr(CO)_3$
1835.4	1795.0	1792.6	1.0225	1.0239	$Cr(CO)_2$ site
1832.9	1792.7	1790.0	1.0224	1.0240	$Cr(CO)_2$, b_2
1762.9					anion
1735.4	1698.9	1693.7	1.0215	1.0246	$Cr_2(CO)_2$, b_2
1705.0	1666.2	1666.7	1.0233	1.0230	$Cr(CO)_2^-$
1678.0	1640.5	1637.7	1.0229	1.0246	$CrCO^-$
1517.4	1484.2	1481.2	1.0224	1.0244	$(CO)_2^-$
1516.2	1483.0	1480.1	1.0224	1.0244	$(CO)_2^-$ site
672.6	659.2	670.0	1.0225	1.0039	$Cr(CO)_6$
430.8	427.3	428.4	1.0082	1.0056	$Cr(CO)_4$

2150.1 cm^{-1} doublet was increased 2-fold, the 2129.8 cm^{-1} was increased by 50%, and the sharp 1666.2 and 1640.5 cm^{-1} bands were reduced to <10% of their yield without CCl_4 added, whereas the 1974.6 cm^{-1} band ($Cr^{13}CO$) was decreased to half.

A diagnostic experiment was carried out with 0.1% ^{12}CO and 0.1% ^{13}CO, and selected spectra are illustrated in Figure 5. The strong 2018.4−1974.6 cm^{-1} doublet, the very strong 1735.4−1715.6−1698.9 cm^{-1} triplet, and the weaker 1832.9−1809.6−1792.2 cm^{-1} triplet are obvious, and a much weaker associated 1982.1−1962.8−1937.0 cm^{-1} triplet and weak 3718.8−3679.2−3637.4 triplet (not shown) are present. Two weak intermediate components are observed at 1856 and 1844 cm^{-1} for the 1873.8 cm^{-1} band, and a single sharp feature is observed at 1681.7 cm^{-1} between the 1705.0 cm^{-1} (obscured by a very strong 1698.9 cm^{-1} absorption) and 1666.2 cm^{-1} bands. The rest of the spectrum is too congested to identify mixed-isotope components for specific higher carbonyls.

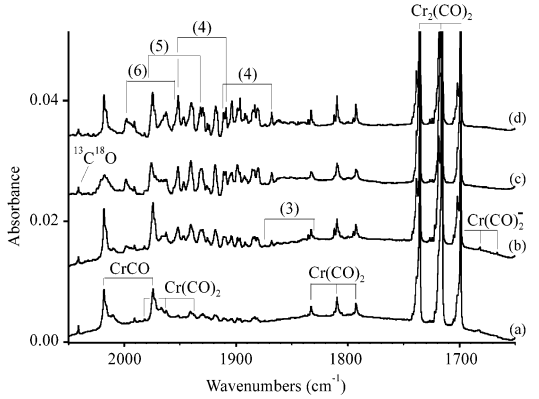

Figure 5. Infrared spectra in the 2050−1650 cm^{-1} region for reduced-energy laser-ablated Cr co-deposited with 0.1% ^{12}CO and 0.1% ^{13}CO in neon at 4 K. Sample deposited (a) for 45 min, (b) after 8 K annealing, (c) after $\lambda > 240$ nm photolysis for 15 min, and (d) after 10 K annealing.

TABLE 3: Calculated (BP86) Geometries, Relative Energies (kcal/mol), Vibrational Frequencies (cm^{-1}), and Infrared Intensities (km/mol) for CrCO, $CrCO^+$, and $CrCO^-$

molecule	relative energy	geometry (Å, deg)	$^{12}C^{16}O$	$^{13}C^{16}O$	$^{12}C^{18}O$
CrCO ($^7A'$)	0	Cr−C: 2.142,	1928.9(993)	1886.2(947)	1882.0(948)
		C−O: 1.162,	327.9(11)	319.5(10)	325.4(12)
		CrCO: 139.7	185.6(17)	183.0(17)	180.2(16)
CrCO ($^5\Pi$)	+6.9	Cr−C: 1.845,	1871.4(678)	1830.3(647)	1827.0(648)
		C−O: 1.183,	493.3(0.4)	481.4(0.5)	488.4(0.3)
		180.0	307.5(26)	303.8(27)	298.3(24)
$CrCO^+$ ($^6\Sigma^+$)	+150.8	Cr−C: 2.057,	2147.8(258)	2099.1(243)	2097.4(251)
		C−O: 1.136,	346.7(1)	342.9(1)	338.9(1)
		180.0	258.9(1)	251.4(1)	255.4(1)
$CrCO^-$ ($^6\Pi$)	−14.8	Cr−C: 1.921,	1718.2(679)	1679.5(628)	1678.1(662)
		C−O: 1.206,	404.8(36)	395.3(33)	400.7(34)
		180.0	231.0(38)	228.1(37)	224.2(36)

TABLE 4: Calculated (B3LYP) Geometries, Relative Energies (kcal/mol), Vibrational Frequencies (cm^{-1}), and Infrared Intensities (km/mol) for CrCO, $CrCO^+$, and $CrCO^-$

molecule	relative energy	geometry (Å, deg)	$^{12}C^{16}O$	$^{13}C^{16}O$	$^{12}C^{18}O$
CrCO ($^7A'$)	0	Cr−C: 2.216,	2015.1(1508)	1970.8(1437)	1965.6(1442)
		C−O: 1.146,	267.8(10)	260.1(9)	266.2(11)
		CrCO: 137.4	177.6(18)	175.7(18)	172.1(17)
$CrCO^+$ ($^6\Sigma^+$)	+143.1	Cr−C: 2.134,	2265.4(237)	2214.2(224)	2211.7(231)
		C−O: 1.120,	298.4(0.7)	295.1(0.6)	291.7(0.5)
		180.0	248.6(0.4)	241.5(0.4)	245.2(0.3)
$CrCO^-$ ($^6\Pi$)	−8.5	Cr−C: 2.007,	1774.2(819)	1733.5(794)	1733.1(764)
		C−O: 1.191,	343.5(17)	339.8(16)	335.6(16)
		180.0	473.7(92)	230.0(86)	233.9(89)

Calculations. DFT calculations were done for the CrCO neutrals, cations, and anions using BP86 and B3LYP functionals to be consistent with previous MCO calculations, and the results are summarized in Tables 3 and 4. Previous calculations have shown that these functionals work well for $Cr(CO)_6$ geometry and vibrational frequencies.[34] As found previously, $^7A'$ is the ground state for CrCO, with $^5\Pi$ higher by 6−9 kcal/mol depending on the calculation.[19−21] The $CrCO^+$ cation has the $^6\Sigma^+$ ground state,[35,36] and the $CrCO^-$ anion has the $^6\Pi$ ground state.

Analogous calculations were done for the $M(CO)_2^{+,o,-}$ species at the BP86 level, and the results are summarized in Tables 5 and 6. The ground state for $Cr(CO)_2$ is found to be $^5\Pi_g$, with $^5A_1$ only 5.1 kcal/mol higher and $^5B_1$, 18 kcal/mol higher. The lowest triplet state, $^3A_2$, is 6.2 kcal/mol higher. The computed $Cr(CO)_2^-$ ground state is $^4\Sigma_g^-$, and the $^4A_2$ state is 6.5 kcal/

TABLE 5: Results of Computations Performed at the BP86/6-311+G* Level of Density Functional Theory on the Linear ($D_{\infty h}$) Configurations of $Cr(CO)_2$ and Its Ions

	$Cr(CO)_2$		$Cr(CO)_2^-$		$Cr(CO)_2^+$
state	$^3\Delta_g$	$^5\Pi_g$	$^4\Sigma_g^-$	$^4\Pi_g$	$^6\Sigma_g^+$
r_e(Cr−C), Å	1.895	1.967	1.886	2.009	2.119
r_e(C−O)	1.173	1.163	1.201	1.142	1.133
$\omega(\pi_u)$[a,b]	67[5]	26[4]	37[2]	69[5]	27[4]
$\omega(\pi_g)$	284[0]	263[0]	254[0]	275[0]	249[0]
$\omega(\sigma_g)$	410[0]	367[0]	410[0]	339[0]	277[0]
$\omega(\sigma_u)$	490[94]	446[68]	506[23]	375[75]	328[35]
$\omega(\pi_u)$	579[1]	410[7]	538[19]	443[3]	287[1]
$\omega(\sigma_u)$	1853 [2794]	1900 [3040]	1691 [3772]	2056 [1496]	2142 [812]
$\omega(\sigma_g)$	1953[0]	2004[0]	1810[0]	2125[0]	2178[0]
E_{rel}[c]	+21.4	0.0	−32.1	+183	+155

[a] Calculated harmonic frequencies, cm^{-1} [intensities, km/mol]. [b] π_u components summed and divided by 2 for both frequencies and intensities. [c] kcal/mol.

mol higher. The $Cr(CO)_2^+$ cation has the $^6\Sigma_g^+$ ground state, in agreement with previous calculations,[36] with a $^4B_2$ state 17 kcal/mol higher. Finally, $Cr(CO)_3$ was calculated, and we find a $^1A_1$ ground state with C_{3v} symmetry, in agreement with previous workers.[8,12,14,37] Computed bond lengths are 1.797 and 1.173 Å, the C−Cr−C angle is 88.6°, the e mode is 1878.4 cm^{-1} (1109 × 2 km/mol), and the a_1 mode is 1972.5 cm^{-1} (187 km/mol). Analogous calculations were done with other functionals to verify the ground state of $Cr(CO)_2$. Of course, BPW91 was virtually the same as BP86. The B3LYP functional gave the same order of states with a 5.8 kcal/mol energy difference and 40−90 cm^{-1} higher C−O stretching frequencies.

Discussion

The unsaturated chromium carbonyl infrared absorptions in solid argon and neon will be assigned by comparison with previous gas-phase[12−14] and matrix-isolation[6−10] work, isotopic substitution, and density functional theory frequency calculations.

CrCO. The first absorption observed at 1977 cm^{-1} in the co-deposition of thermal Cr atoms and CO under dilute conditions has been assigned to CrCO.[10] The first absorption at 1975.6 cm^{-1} in dilute laser-ablated Cr experiments (Figure 1) is likewise due to CrCO (the frequency difference is in the grating infrared spectrometer measurement, not the method of generating Cr atoms). The first absorption to appear in this region in solid neon at 2018.4 cm^{-1} also shows the doublet characteristic of one carbon atom (one CO submolecule), which substantiates the assignment to CrCO.

This assignment to CrCO is supported by previous and present DFT calculations, which find a high-spin $^7A'$ ground state.[19−21] The B3LYP functional works better than pure DFT for computing the frequency (2015.1 cm^{-1}) of CrCO, and the 2018.4 cm^{-1} neon matrix frequency is a better prediction of the yet-to-be observed gas-phase fundamental.

The argon-to-neon matrix shift for CrCO is unusually large, 42.8 cm^{-1}.[22,38] However, this is a high-spin ($^7A'$) species, and the potential for interaction with the noble gas host is high for CrCO with only one "ligand" present. The higher carbonyls, even $Cr(CO)_2$, have much smaller argon-to-neon matrix shifts (11−14 cm^{-1}). CrO ($^5\Pi$) also exhibits a large (33.9 cm^{-1}) argon-to-neon matrix shift.[25,39]

$Cr(CO)_2$. The next band observed to gain intensity on first annealing to 20 K in solid argon is at 1821.5 cm^{-1}. Annealing to 25 K produces more of the 1821.5 cm^{-1} band in an associated weaker 1970.8 cm^{-1} absorption with 8:1 relative intensity. The 1970.8 and 1821.5 cm^{-1} absorptions form sharp 1:2:1 triplet patterns with the $^{12}CO/^{13}CO$ mixture, which indicates the vibration of two equivalent C−O subgroups. The weaker 1970.8 cm^{-1} band is assigned to the symmetric (a_1), and the stronger 1821.5 cm^{-1} band, to the antisymmetric (b_2) C−O stretching mode in $Cr(CO)_2$. The 1951.3 cm^{-1} intermediate component is 3.0 cm^{-1} above the median, and the 1798.4 cm^{-1} intermediate component is 3.0 cm^{-1} below the median of the $Cr(^{12}CO)_2$ and $Cr(^{13}CO)_2$ bands. This demonstrates that these two absorptions are due to the same molecule, as the two mixed-isotope $Cr(^{12}CO)(^{13}CO)$ stretching modes interact due to symmetry lowering. Similar triplet absorptions are observed in solid neon for the 1832.9 and 1982.1 cm^{-1} bands (5:1 relative intensity) for the b_2 and a_1 stretching modes of $Cr(CO)_2$. In this case, the intermediate components are 3.2 cm^{-1} below and above the pure isotopic median bands, demonstrating a weak interaction between two fundamentals of the mixed-isotope $Cr(^{12}CO)(^{13}CO)$ molecule and confirming the association of these two stretching fundamentals with the same $Cr(CO)_2$ molecule. In addition, the $^{12}CO/^{13}CO$ and $C^{16}O/C^{18}O$ isotopic frequency ratios, 1.0224 and 1.0240, respectively, for b_2 and 1.0233 and 1.0231 for a_1 in neon reveal a slight difference in these normal modes, as expected. Note that the $(a_1)-(b_2)$ mode separation is the same, 149.2 ± 0.1 cm^{-1}, in both the argon and neon matrices,

TABLE 6: Results of Computations Performed at the BP86/6-311+G* Level of Density Functional Theory on the Bent (C_{2v}) Configurations of $Cr(CO)_2$ and Its Ions

	$Cr(CO)_2$			$Cr(CO)_2^-$			$Cr(CO)_2^+$	
state	$^1A_2$	$^3A_2$	$^5A_1$	$^2A_1$	$^4A_2$	$^6A_1$[a]	$^2A_2$	$^4B_2$
r_e(Cr−C), Å	1.793	1.799	1.922	1.761	1.816	1.932	1.865	1.916
r_e(C−O)	1.178	1.179	1.168	1.207	1.199	1.185	1.150	1.146
∠CCrC, deg	77.2	76.9	108.3	85.8	70.9	104.5	81.9	90.0
∠CrCO	176.6	176.8	174.7	178.7	179.2	179.0	178.7	179.4
$\omega(a_1)$[b]	109[2]	107[2]	65[1]	93[0]	108[1]	57[2]	100[2]	90[2]
$\omega(a_2)$	356[0]	360[0]	209[0]	352[0]	375[0]	171[0]	333[0]	299[0]
$\omega(b_1)$	391[14]	389[15]	278[6]	373[1]	365[31]	170[279]	351[4]	310[1]
$\omega(b_2)$	432[7]	433[6]	322[3]	425[2]	440[66]	304[7]	368[2]	340[3]
$\omega(a_1)$	537[0]	529[0]	415[0]	546[0]	516[11]	407[1]	425[36]	416[0]
$\omega(b_2)$	520[19]	520[19]	442[52]	575[8]	503[58]	439[3]	440[1]	431[15]
$\omega(a_1)$	646[1]	634[0]	474[0]	679[15]	569[53]	489[1]	579[1]	562[0]
$\omega(b_2)$	1815 [1066]	1808 [1157]	1881 [1911]	1704 [1172]	1696 [1465]	1778 [1415]	1990 [812]	2038 [519]
$\omega(a_1)$	1922 [521]	1923 [471]	1962 [283]	1759 [1643]	1806 [981]	1844 [871]	2060 [194]	2096 [144]
E_{rel}[c]	14.5	6.2	5.1	−21.0	−25.6	−20.5	+191	+172

[a] The lowest $^6A_1$ cation state converged to the linear $^6\Sigma_g^+$ state. [b] Calculated harmonic frequencies, cm^{-1} [intensities, km/mol]. [c] kcal/mol; differences in the total energy with respect to the neutral calculated $^5\Pi_g$ ground state.

indicating the same bent structure since an angle change would alter the stretch−stretch interaction and mode separation.

This assignment to $Cr(CO)_2$ is supported by our DFT calculations, which predict a $^5\Pi_g$ ground state with a σ_u mode at 1900 cm^{-1}, an inactive σ_g mode at 2004 cm^{-1}, and a 5.1 kcal/mol higher $^5A_1$ state with stretching frequencies at 1962 and 1881 cm^{-1} and a 1:7 relative intensity (BP86) and at 2055 and 1925 cm^{-1} with a 1:12 relative intensity (B3LYP). The $^5A_1$ state frequencies are in reasonable agreement with our observations. However, the 6.2 kcal/mol higher $^3A_2$ state frequencies are both computed to be lower than the observed bands. There are two possibilities: (a) our DFT calculations are accurate enough to confirm a linear ground state for the gas-phase $Cr(CO)_2$ molecule, and matrix interaction with the Cr center lowers the $^5A_1$ state energy more than the linear state energy such that the bent state is in the ground state in solid argon and neon or (b) the calculated energies are not accurate to the 5.1 kcal/mol difference and a more accurate calculation will find that $^5A_1$ is the ground state in both the gas and matrix phases. The observation of two C−O stretching modes confirms the trapping of a bent structure, and the excellent fit between the BP86-predicted $^5A_1$ state and the neon matrix frequencies identifies this state.

A weak band that appeared at 1903 cm^{-1} on prolonged photolysis of $Cr(CO)_6$ in solid CH_4 has been provisionally assigned to $Cr(CO)_2$ by Turner et al.[8] The transient absorption at 1914 cm^{-1} in the gas-phase photodissociation of $Cr(CO)_6$ has also been attributed to $Cr(CO)_2$ by Weitz et al., who noted that this frequency is rather high.[12] Both of these associations with $Cr(CO)_2$ are in error unless the gas-phase absorption is due to an excited state. By the time four CO subunits are removed from $Cr(CO)_6$, the chemistry is complicated. The best model for $Cr(CO)_2$ in the gas phase is our strong neon matrix absorption at 1833 cm^{-1}. Even if the molecule is linear in the gas phase, the calculations suggest that the antisymmetric fundamental is only 20 cm^{-1} higher for the linear molecule. Thus, in either case, the gaseous $Cr(CO)_2$ molecule should absorb strongly near 1850 cm^{-1}.

$Cr(CO)_n$ (n = 3, 4, 5). The matrix and gas-phase results are all in agreement on the higher binary unsaturated Cr carbonyl species. Fundamentals reported by the Turner group[8,9] for the higher $Cr(CO)_n$ (n = 3, 4, 5) species in solid argon using the photodissociation of $Cr(CO)_6$ agree within ±2 cm^{-1} with our measurements using reactions of laser-ablated Cr atoms and CO. The present neon matrix observations are completely compatible with the argon matrix spectra, where 9−16 cm^{-1} blue shifts are observed from argon to neon. Furthermore, the neon matrix fundamentals are between the gas-phase and argon matrix values. For example, the antisymmetric C−O stretching modes of $Cr(CO)_4$ are 1957, 1920 cm^{-1} in gas,[12] 1952, 1911 cm^{-1} in neon, and 1939, 1895 cm^{-1} in the argon matrix. In addition, several low-frequency fundamentals can be associated with carbonyl stretching modes on annealing in the argon matrix experiments. These bands and possible assignments are listed in Table 2. Similar absorptions were reported by Graham et al.[4] The weak bands assigned to $Cr(CO)_3$ are in agreement with intervals from the photoelectron spectrum of $Cr(CO)_3$.[37]

The saturated $Cr(CO)_6$ molecule is also formed here with the same triply degenerate modes (±1 cm^{-1}) as in the authentic material.[6,32] We note that one Ar atom complexed to $Cr(CO)_6$ reduces the strong mode from 2002.94 to 2002.2 cm^{-1}.[40] Our BP86 calculations for $Cr(CO)_3$ predict a degenerate fundamental at 1878.4 cm^{-1} in excellent agreement with the 1873.8 cm^{-1} neon matrix observation and a symmetric fundamental at 1972.5 cm^{-1} in very good agreement with the 1979 cm^{-1} methane matrix assignment[8] and the 2000 ± 10 cm^{-1} interval from the photoelectron spectrum of $Cr(CO)_3^-$.[37]

$CrCO^+$. A unique contribution of the neon matrix work is new data on molecular ions. There is a sharp, weak 2200.7, 2199.2 cm^{-1} doublet with ^{12}CO shifted to 2151.9, 2150.1 cm^{-1} with ^{13}CO. These bands were increased by 2−3-fold upon doping with CCl_4 to capture ablated electrons (Figure 4), whereas the CrCO yield was reduced to half. This is the behavior expected and observed for positive ions as CCl_4 captures ablated electrons and fosters the survival of ablated cations.[22,33] Hence, the 2200.7 cm^{-1} band is assigned to the C−O fundamental of $CrCO^+$.

Our assignment to $CrCO^+$ is confirmed by DFT frequency calculations for the $^6\Sigma^+$ ground state. The B3LYP and BP86 functionals predict 250 and 219 cm^{-1} higher fundamentals for the cation than the neutral, respectively, and our observed frequency is 182 cm^{-1} higher. Ab initio calculations confirm the $^6\Sigma^+$ ground state, predict a 13 kcal/mol binding energy for $CrCO^+$, find primarily an electrostatic interaction, and predict a higher frequency.[35,36]

$Cr(CO)_2^+$. Sequential bond energies determined for the $Cr(CO)_x^+$ series of cations[41,42] suggest that higher carbonyl cations could also be observed here and that the 2178.1 cm^{-1} absorption increases with added CCl_4, increases on annealing, exhibits the proper isotopic shifts for a carbonyl vibration, and is therefore assigned to $Cr(CO)_2^+$. The weaker 2172.2 cm^{-1} absorption is markedly increased on annealing and on the addition of CCl_4 and is probably due to $Cr(CO)_3^+$. Likewise, the new 2167.6 and 2162.0 cm^{-1} bands, which behave similarly, are probably due to higher carbonyl cations, but without isotopic, data we cannot be certain. The $(CO)_2^+$ cation[43] is observed at 2056.3 cm^{-1} in these experiments.

We find a $^6\Sigma_g^+$ ground state for $Cr(CO)_2^+$, in agreement with previous work,[36] with strong σ_u fundamental predicted at 2142 cm^{-1}, just 6 cm^{-1} below $CrCO^+$, at the BP86 level of theory. This is in accord with the experimental difference of 22 cm^{-1}. Obviously, the BP86 calculation underestimates the $Cr(CO)_2^+$ fundamental (by 36 cm^{-1}), but the next lowest $^4B_2$ state has an even lower b_2 mode at 2038 cm^{-1}, which is not compatible with the observed spectrum.

$Cr(CO)_2^-$. The sharp 1705.0 cm^{-1} band in neon and the 1688.0 cm^{-1} argon counterpart were destroyed by $\lambda > 470$ nm irradiation. With CCl_4 added to capture ablated electrons, the 1705.0 cm^{-1} band was essentially absent from the spectrum, which suggests the identification of an anion.[22,33] Both matrices reveal triplet mixed-isotope bands, and this shows that two equivalent CO subunits are involved in this vibrational mode. The assignment of these bands to the antisymmetric C−O stretching mode of $Cr(CO)_2^-$ is confirmed by DFT calculations, which find a $^4\Sigma_g^-$ ground state with very intense σ_u mode at 1691 cm^{-1} (BP86). The bent $^4A_2$ anion state is only 6.5 kcal/mol higher, and the computed b_2 frequency is nearly the same as that observed, but we fail to observe the predicted a_1 mode. All of this evidence supports the $^4\Sigma_g^-$ ground state for the $Cr(CO)_2^-$ anion observed here. We note that the DFT computed electron affinity for $Cr(CO)_2$, 32.1 kcal/mol (BP86), is nearly the same as the experimental measurement for $Cr(CO)_3$ (31.1 kcal/mol).[37] This is in accord with photobleaching using $\lambda > 800$ nm light.

The flowing afterglow experiment[37,44] with $Cr(CO)_6$ also revealed three photoelectron bands for $Cr(CO)_2^-$. These bands are difficult to interpret in part because of the possibility of excited-state $Cr(CO)_2^-$ precursors. A band at 0.76 ± 0.01 eV

electron kinetic energy exhibited a single 1960 ± 20 cm^{-1} vibrational interval for a symmetric C−O stretching mode in a neutral $Cr(CO)_2$ state. This is in acceptable agreement with the present neon matrix observation (1982.1 cm^{-1}) for $Cr(CO)_2$.

The weak 1762.9 and 1678.0 cm^{-1} absorptions could be due to anions since these photosensitive bands were not observed with CCl_4 dopant. Our DFT calculations predict a $^6\Pi$ ground state for $CrCO^-$ with a strong 1718.2 cm^{-1} fundamental, and the 1678.0 cm^{-1} absorption is a reasonable assignment. Unfortunately, no isotopic data are available for the 1762.9 cm^{-1} band owing to masking by very strong $Cr_2(CO)_2$ absorptions. This absorption could be due to $Cr(CO)_3^-$, which has been observed in the gas phase,[37] but we cannot be certain. Full-arc radiation increased the yield of $Cr(CO)_5$ and produced weak new absorptions at 1856.7, 1838.4 cm^{-1} in solid argon near those assigned to $Cr(CO)_5^-$ by Breeze et al.[45] In addition, some $Cr(CO)_2^-$ absorption was restored, and weak absorptions increased at 1809.6 and 1787.4 cm^{-1}. The latter absorptions are probably due to higher $Cr_x(CO)_y$ species (Figure 1e).

$Cr_2(CO)_2$. The strongest absorption observed here, even with reduced laser energy, is the sharp 1735.4 cm^{-1} band, and the 1715.6 cm^{-1} mixed-isotope counterpart is observed from ^{13}CO in natural abundance in solid neon (Figure 3). This absorption increases on annealing and is followed by weaker sharp bands at 1938.6, 3718.8, and 3912.4 cm^{-1}. These bands exhibit 1:2:1 triplet absorptions with mixed $^{12}CO/^{13}CO$ (intermediate components at 1715.6, 1917.0, and 3870.2 cm^{-1}, respectively), indicating that two equivalent CO subunits participate in these modes. Increased laser energy favors this band relative to CrCO in nearly second order, and the $(CrCO)_2$ dimer (i.e., $Cr(\mu\text{-}CO)_2Cr$) is the most likely absorber. Hence, the 1715.6 cm^{-1} absorption is due to $Cr_2(^{12}CO)(^{13}CO)$ in natural abundance. Note that the 1735.4 cm^{-1} fundamental is in the bridging carbonyl stretching region.[46] The major site absorption shows only a 1.4 cm^{-1} argon-to-neon matrix shift.

The strong 1735.4 cm^{-1} absorption exhibits decreased $^{12}CO/^{13}CO$ and increased $C^{16}O/C^{18}O$ frequency ratios, 1.0215 and 1.0246, relative to CO itself, which is characteristic of an antisymmetric C−O stretching mode (compare $Cr(CO)_2$). The intermediate components for $Cr_2(^{12}CO)(^{13}CO)$ and $Cr_2(C^{16}O)(C^{18}O)$ at 1715.6 and 1712.8 cm^{-1} are 1.6 and 1.8 cm^{-1}, respectively, lower than the means of pure isotopic frequencies, which points to a higher-frequency symmetric C−O stretching mode. The $Cr_2(^{12}C^{18}O)(^{13}C^{18}O)$ counterpart of the antisymmetric mode was also observed at 1673.2 cm^{-1}.

The sharp, weaker 1938.6 cm^{-1} absorption is 203.2 cm^{-1} above the strong 1735.4 cm^{-1} band, and the ^{13}CO counterpart is separated by 197.6 cm^{-1} and the $C^{18}O$ counterpart, by 198.7 cm^{-1}. These intervals are probably due to a low-frequency deformation mode. The next combination band at 3718.8 cm^{-1} is separated from the 1938.6 cm^{-1} band by 1780.2 cm^{-1}. Analogous separations of 1740.9 and 1741.5 cm^{-1} for the ^{13}CO and $C^{18}O$ bands, respectively, are appropriate for a symmetric C−O stretching mode. The final combination band at 3912.4 cm^{-1} is 193.6 cm^{-1} above the 3718.8 cm^{-1} band, and this interval, allowing for increased anharmonicity, is probably due to the same mode as the first 203.2 cm^{-1} interval. Hence, the 3912.4 cm^{-1} band is probably due to the sum of a_1 and b_2 C−O fundamentals and 2× the low a_1 mode.

Using $Ni(CO)_2$ as a model where both fundamentals and a combination are observed[47] and the sum of fundamentals is 25 cm^{-1} higher than the combination band, we predict the symmetric C−O stretching mode of $Cr_2(CO)_2$ to be some 20 cm^{-1} higher, near 1800 cm^{-1}. A sharp, weak band at 1810 cm^{-1} could be due to this mode, but we cannot be certain.

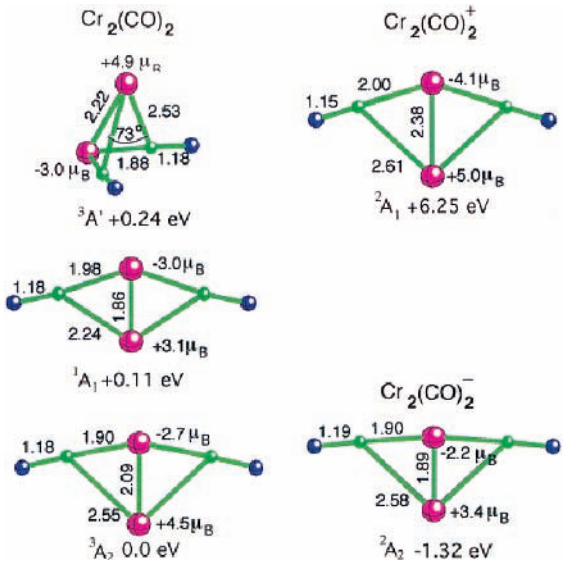

Figure 6. Structures of the lowest-energy states of $Cr_2(CO)_2$ and its ions calculated at the BPW91/6-311+G* level. Bond lengths are in angstroms, and excess spin densities on Cr sites are in Bohr magnetons.

TABLE 7: Results of Calculations Performed at the BPW91/6-311+G* Level of Density Functional Theory for $Cr_2(CO)_2$ and Its Ions

	$Cr_2(CO)_2$			$Cr_2(CO)_2^-$	$Cr_2(CO)_2^+$
	$^1A_1$	$^3A_2$	$^3A'$	$^2A_2$	$^2A_1$
$\omega(b_1)$ cm^{-1}	47[6]	46[3]	22[0][a]	40[2]	34[5]
$\omega(a_1)$	101[1]	74[1]	57[5]	68[3]	75[1]
$\omega(a_1)$	157[12]	142[1]	92[1]	251[20]	160[0]
$\omega(b_2)$	167[4]	82[0]	171[1]	88[1]	71[2]
$\omega(a_2)$	241[0]	301[0]	229[3]	309[0]	269[0]
$\omega(a_1)$	336[1]	404[3]	344[1]	397[69]	323[7]
$\omega(b_1)$	374[2]	520[3]	369[2]	519[16]	318[1]
$\omega(a_1)$	386[2]	440[0]	437[11]	423[21]	396[0]
$\omega(b_2)$	390[67]	332[5]	477[39]	408[6]	305[15]
$\omega(b_2)$	441[1]	491[50]	502[0]	493[16]	416[22]
$\omega(b_2)$	1845 [1856]	1833 [2308]	1812 [1655]	1748 [2347]	2001 [1371]
$\omega(a_1)$	1872 [15]	1905 [81]	1867 [529]	1802 [343]	2025 [56]
μ, debye	0.74	0.74	3.17		
E_{rel}, eV	+0.11	0.0	+0.24	−1.32	+6.25

[a] $\omega(a')$ and $\omega(a'')$.

Accordingly, extensive DFT calculations were made for $Cr(\mu\text{-}CO)_2Cr$ in odd spin multiplicities from 1 to 13, the anion in even multiplicities from 2 to 12 and the cation, from 2 to 10. The lowest-energy states converged in C_{2v} symmetry with two equivalent CO subunits and two nonequivalent Cr atoms ($^3A_2$), and the $^1A_1$ and $^3A'$ structures are illustrated in Figure 6. The ions gave $^2A_2$ states that suggest a singlet or triplet ground state for $Cr_2(CO)_2$ at the DFT level of theory.

The very strong b_2 fundamental calculated for the $^3A_2$ state at 1833 cm^{-1} (Table 7) is almost 100 cm^{-1} higher than the strong fundamental observed 1735 cm^{-1}. Recall that the BP86 calculation was almost 50 cm^{-1} too high for $Cr(CO)_2$. The inclusion of anharmonicity would reduce the calculated harmonic frequency additionally by approximately 20 cm^{-1}, so considering the known difficulty in calculating dichromium itself,[48] our $Cr_2(CO)_2$ calculations are approximate at best, and the agreement is acceptable.

However, the density functional may favor lower spin states. We find that the strong antisymmetric fundamental ranges from 1867 to 1694 cm^{-1} for odd spin multiplicities from 1 to 13 and that the energy increases to +39 kcal/mol. It is possible that a

more rigorous calculation will find a higher spin ground state for $Cr_2(CO)_2$.

Several other absorptions in these experiments are favored by higher laser energy and are likely due to polynuclear chromium carbonyls. These include bands at 1940.9, 1926.0, and 1892.0 cm^{-1} labeled $Cr_x(CO)_y$ in Table 2. The latter band shifts to 1878.5 cm^{-1} in solid argon and exhibits a sharp doublet with mixed $^{12}CO/^{13}CO$, but weaker intermediate components could be masked by $Cr(CO)_3$ isotopic absorptions.

Reaction Mechanisms. Several comparisons are of interest. First, Cr atoms react with CO on co-deposition with excess argon and neon and on annealing the solid samples to form all of the $Cr(CO)_n$ ($n = 1-6$) carbonyls. The first high-spin reaction proceeds readily, and the second reaction occurs on annealing solid neon to 6 K and solid argon to 20 K (Figures 1 and 3) despite the spin change. However, the third reaction appears to be slower, as the spin change is greater and the yield of $Cr(CO)_3$ is smaller in both matrices.

$$Cr(^7S) + CO(^1\Sigma^+) \rightarrow CrCO(^7A') \quad (1)$$

$$CrCO(^7A') + CO(^1\Sigma^+) \rightarrow Cr(CO)_2(^5A_1) \quad (2)$$

$$Cr(CO)_2(^5A_1) + CO(^1\Sigma^+) \rightarrow Cr(CO)_3(^1A_1) \quad (3)$$

The $Cr(CO)_4$ absorptions are stronger in accord with a fast fourth reaction, as observed in the gas phase[12-14] with no spin change. Likewise, the fifth and sixth reactions are favorable.

$$Cr(CO)_3 + CO \rightarrow Cr(CO)_4 \text{ (all singlets)} \quad (4)$$

$$Cr(CO)_4 + CO \rightarrow Cr(CO)_5 \text{ (all singlets)} \quad (5)$$

$$Cr(CO)_5 + CO \rightarrow Cr(CO)_6 \text{ (all singlets)} \quad (6)$$

Note that the $Cr(CO)_{5,6}$ absorptions are stronger in neon after 10 K annealing than in argon after 40 K annealing, as more CO diffusion occurs in the former than in the latter. Likewise, reactions occuring on co-deposition in neon at 4 K are stronger than those in argon at 10 K because the neon sample is frozen more slowly and accordingly more diffusion and reaction of CO can take place.

We note that ground-state (^7S) Cr atoms in the gas phase are unreactive with CO, which was attributed to spin restrictions arising from the ^7S state of Cr.[49] However, CrCO increases on annealing in solid neon, so reaction 1 will proceed if the orientation of Cr and CO allow the bent $^7A'$ CrCO state to be formed and the new complex is relaxed. The matrix environment provides both of these requirements that are lacking in the gas phase.

The laser-ablation process produces cations and electrons.[22,33,50] Laser-ablated Cr^+ also reacts with CO to give the chromium carbonyl cation.

$$Cr^+(^6S) + CO(^1\Sigma^+) \rightarrow CrCO^+(^6\Sigma^+) \quad (7)$$

$$CrCO^+(^6\Sigma^+) + CO(^1\Sigma^+) \rightarrow Cr(CO)_2^+(^6\Sigma_g^+) \quad (8)$$

This reaction occurs on deposition and on diffusion of trapped species (Figure 4). Successive carbonyls are bound to the metal cation center,[41,42] and annealing produces higher carbonyl cations. The role of CCl_4 is to capture ablated electrons, thus facilitating the survival of more Cr^+ and $CrCO^+$ and reducing the yield of carbonyl product anions.[22,33] Hence, electrons are intercepted by CCl_4, and the favorable chromium dicarbonyl electron-capture process is minimized upon the addition of CCl_4. Ultraviolet irradiation photodetaches the $Cr(CO)_2^-$ anion and photoneutralizes the cation (Figure 4). However, the $Cr(CO)_5^-$ anion is more stable and survives photolysis.[45]

$$Cr(CO)_2(^5A_1) + e^- \rightarrow Cr(CO)_2^-(^4\Sigma_g^-) \quad (9)$$

Polynuclear chromium species are also observed in these experiments, particularly in the more slowly condensing neon matrix. The strongest absorption observed here is from a bridged dicarbonyl, most likely with two nonequivalent chromium atoms formed from the dimerization of CrCO, which is exothermic by 60 kcal/mol (BP86).

$$2CrCO(^7A') \rightarrow Cr_2(CO)_2(^3A_2) \quad (10)$$

Conclusions

Laser-ablated Cr atoms react with CO in excess argon to give the same $Cr(CO)_{3,4,5}$ species observed from the photodissociation of $Cr(CO)_6$. The neon matrix fundamentals of these intermediate species are between argon matrix and gas-phase values. The dicarbonyl $Cr(CO)_2$ is bent with 1970.8, 1821.5 cm^{-1} and 1982.1, 1832.9 cm^{-1} C−O stretching fundamentals in solid argon and neon, respectively. The high-spin CrCO molecule appears at 1975.6 and 2018.4 cm^{-1} in solid argon and neon, respectively, and exhibits a strong matrix interaction. The polynuclear $Cr_2(CO)_2$ complex absorbs at 1735.4 cm^{-1} and gives several combination bands in solid neon. The $CrCO^+$ cation and $Cr(CO)_2^-$ anion are observed in solid neon at 2200.7 and 1705.0 cm^{-1}, respectively, using laser ablation, which produces cations and electrons. Density functional theory calculations suggest ground-state structures and support the vibrational assignments.

Acknowledgment. We gratefully acknowledge support for this work from NSF grants CHE97-00116 and CHE00-78836 and NASA grant NCC 2-5415 and helpful correspondence with C. W. Bauschlicher, Jr., D. G. Leopold, and R. N. Perutz.

References and Notes

(1) Cotton, F. A.; Wilkinson, G.; Murillo, C. A.; Bochmann, M. *Advanced Inorganic Chemistry*, 6th ed.; Wiley & Sons: New York, 1999.
(2) Collman, J. P.; Hegedus, L. S.; Norton, J. R.; Fink, R. G. *Principles and Applications of Organotransition Metal Chemistry*; University Science Books: Mill Valley, CA, 1987.
(3) Hoffmann, R. *Angew. Chem., Int. Ed. Engl.* **1982**, *21*, 711.
(4) Graham, M. A.; Poliakoff, M.; Turner, J. J. *J. Chem. Soc. A* **1971**, 2939.
(5) Kundig, E. P.; Ozin, G. A. *J. Am. Chem. Soc.* **1974**, *96*, 3820.
(6) Perutz, R. N.; Turner, J. J. *Inorg. Chem.* **1975**, *14*, 262.
(7) Perutz, R. N.; Turner, J. J. *J. Am. Chem. Soc.* **1975**, *97*, 4791.
(8) (a) Perutz, R. N.; Turner, J. J. *J. Am. Chem. Soc.* **1975**, *97*, 4800. (b) Perutz, R. N. Ph.D. Thesis, University of Cambridge, Cambridge, U.K., 1974.
(9) Burdett, J. K.; Graham, M. A.; Perutz, R. N.; Poliakoff, M.; Rest, A. J.; Turner, J. J.; Turner, R. F. *J. Am. Chem. Soc.* **1975**, *97*, 4805.
(10) Bach, S. B. H.; Taylor, C. A.; Van Zee, R. J.; Vala, M. T.; Weltner, W., Jr. *J. Am. Chem. Soc.* **1986**, *108*, 7104.
(11) Church, S. P.; Hermann, H.; Grevels, F. W.; Shaffner, K. *J. Chem. Soc., Chem. Commun.* **1984**, 785.
(12) (a) Seder, T. A.; Church, S. P.; Weitz, E. *J. Am. Chem. Soc.* **1986**, *108*, 4721. (b) Weitz, E. *J. Phys. Chem.* **1987**, *91*, 3945. Weitz, E. *J. Phys. Chem.* **1994**, *98*, 11256.
(13) Fletcher, T. R.; Rosenfeld, R. N. *J. Am. Chem. Soc.* **1985**, *107*, 2203.
(14) (a) Ishikawa, Y.; Brown, C. E.; Hackett, P. A.; Rayner, D. M. *J. Phys. Chem.* **1990**, *94*, 2404. (b) Rayner, D. M.; Ishikawa, Y.; Brown, C. E.; Hackett, P. A. *J. Chem. Phys.* **1991**, *94*, 5471.
(15) Tyndall, G. W.; Jackson, R. L. *J. Chem. Phys.* **1989**, *91*, 2881.

(16) King, J. C.; Zhang, J. Z.; Schwartz, B. J.; Harris, C. B. *J. Chem. Phys.* **1993**, *99*, 7595.
(17) Hassanzadeh, P.; Andrews, L. *J. Phys. Chem.* **1992**, *96*, 9177.
(18) Souter, P. F.; Andrews, L. *J. Am. Chem. Soc.* **1995**, *117*, 7350 (Cr + CO_2, CO).
(19) (a) Fournier, R. *J. Chem. Phys.* **1993**, *98*, 8041. (b) Fournier, R. *J. Chem. Phys.* **1993**, *99*, 1801.
(20) Adamo, C.; Lelj, F. *J. Chem. Phys.* **1995**, *103*, 10605. Adamo, C.; Lelj, F. *Chem. Phys. Lett.* **1995**, *246*, 463.
(21) Gutsev, G. L.; Andrews, L.; Bauschlicher, C. W., Jr., in press.
(22) Zhou, M. F.; Andrews, L.; Bauschlicher, C. W., Jr. *Chem. Rev.* **2001**, *101*, 1931.
(23) Burkholder, T. R.; Andrews, L. *J. Chem. Phys.* **1991**, *95*, 8697.
(24) Hassanzadeh, P.; Andrews, L. *J. Phys. Chem.* **1992,** *96*, 9177.
(25) Zhou, M. F.; Andrews, L. *J. Chem. Phys.* **1999**, *111*, 4230.
(26) Frisch, M. J.; Trucks, G. W.; Schlegel, H. B.; Scuseria, G. E.; Robb, M. A.; Cheeseman, J. R.; Zakrzewski, V. G.; Montgomery, J. A., Jr.; Stratmann, R. E.; Burant, J. C.; Dapprich, S.; Millam, J. M.; Daniels, A. D.; Kudin, K. N.; Strain, M. C.; Farkas, O.; Tomasi, J.; Barone, V.; Cossi, M.; Cammi, R.; Mennucci, B.; Pomelli, C.; Adamo, C.; Clifford, S.; Ochterski, J.; Petersson, G. A.; Ayala, P. Y.; Cui, Q.; Morokuma, K.; Malick, D. K.; Rabuck, A. D.; Raghavachari, K.; Foresman, J. B.; Cioslowski, J.; Ortiz, J. V.; Stefanov, B. B.; Liu, G.; Liashenko, A.; Piskorz, P.; Komaromi, I.; Gomperts, R.; Martin, R. L.; Fox, D. J.; Keith, T.; Al-Laham, M. A.; Peng, C. Y.; Nanayakkara, A.; Gonzalez, C.; Challacombe, M.; Gill, P. M. W.; Johnson, B. G.; Chen, W.; Wong, M. W.; Andres, J. L.; Head-Gordon, M.; Replogle, E. S.; Pople, J. A. *Gaussian 98*, revision A.6; Gaussian, Inc.: Pittsburgh, PA, 1998.
(27) (a) Becke, A. D. *Phys. Rev. A* **1988**, *38*, 3098. (b) Perdew J. P. *Phys. Rev. B* **1983**, *33*, 8822. (c) Perdew, J. P.; Wang, Y. *Phys. Rev. B* **1992**, *45*, 13244.
(28) (a) Becke, A. D. *J. Chem. Phys.* **1993**, *98*, 5648. (b) Stevens, P. J.; Devlin, F. J.; Chablowski, C. F.; Frisch, M. J. *J. Phys. Chem.* **1994**, *98*, 11623.
(29) (a) Krishnan, R.; Binkley, J. S.; Seeger, R.; Pople, J. A. *J. Chem. Phys.* **1980**, *72*, 650. (b) McLean, A. D.; Chandler, G. S. *J. Chem. Phys.* **1980**, *72*, 5639. (c) Frisch, M. J.; Pople, J. A.; Binkley, J. S. *J. Chem. Phys.* **1984**, *80*, 3265.
(30) (a) Wachters, H. J. H. *J. Chem. Phys.* **1970**, *52*, 1033. (b) Hay, P. J. *J. Chem. Phys.* **1977**, *66*, 4377. (c) Raghavachari, K.; Trucks, G. W. *J. Chem. Phys.* **1989**, *91*, 1062.
(31) Darling, J. H.; Ogden, J. S. *J. Chem. Soc., Dalton Trans.* **1972**, 2496.
(32) Jones, L. H.; McDowell, R. S.; Goldblatt, M. *Inorg. Chem.* **1969**, *8*, 2349.
(33) Liang, B.; Zhou, M. F.; Andrews, L. *J. Phys. Chem. A* **2000**, *104*, 3905.
(34) Spears, K. G. *J. Phys. Chem. A* **1997**, *101*, 6273.
(35) Mavridis, A.; Harrison, J. F.; Allison, J. *J. Am. Chem. Soc.* **1989**, *111*, 2482.
(36) Barnes, L. A.; Rosi, M.; Bauschlicher, C. W., Jr. *J. Chem. Phys.* **1990**, *93*, 609.
(37) Bengali, A. A.; Casey, S. M.; Cheng, C. L.; Dick, J. P.; Fenn, P. T.; Villalta, P. W.; Leopold, D. G. *J. Am. Chem. Soc.* **1992**, *114*, 5257.
(38) Jacox, M. E. *Chem. Phys.* **1994**, *189*, 149.
(39) Chertihin, G. V.; Bare, W. D.; Andrews, L. *J. Chem. Phys.* **1997**, *107*, 2798.
(40) Hansford, G. M.; Davies, P. B. *J. Mol. Spectrosc.* **1994**, *168*, 540. Hansford, G. M.; Davies, P. B. *J. Chem. Phys.* **1996**, *104*, 8292.
(41) Khan, F. A.; Clemmer, D. E.; Shultz, R. H.; Armentrout, P. B. *J. Phys. Chem.* **1993**, *97*, 7978.
(42) Chen, Y.-J.; Liao, C.-L.; Ng, C. Y. *J. Chem. Phys.* **1997**, *107*, 4527.
(43) Thompson, W. E.; Jacox, M. E. *J. Chem. Phys.* **1991**, *95*, 735.
(44) Leopold, D. Personal communication, 1998. Bengali, A. A. Ph.D. Thesis, University of Minnesota, Minneapolis, MN, 1992.
(45) Breeze, P. A.; Burdett, J. K.; Turner, J. J. *Inorg. Chem.* **1981**, *20*, 3369.
(46) Himmel, H.-J.; Downs, A. J.; Green, J. C.; Greene, T. M. *J. Phys. Chem. A* **2000**, *104*, 3642.
(47) Manceron, L.; Alikhani, M. E. *Chem. Phys.* **1999**, *244*, 215.
(48) (a) Yanagisawa, S.; Tsuneda, T.; Hirao, K. *J. Chem. Phys.* **2000**, *112*, 545. (b) Barden, C. J.; Rienstra-Kiracofe, C.; Schaefer, H. F., III. *J. Chem. Phys.* **2000**, *113*, 690.
(49) Parnis, J. M.; Mitchell, S. A.; Hackett, P. A. *J. Phys. Chem.* **1990**, *94*, 8152.
(50) Kang, H.; Beauchamp, J. L. *J. Phys. Chem.* **1985**, *89*, 3364.